Journal of Aerosol Science 79 (2015) 48–60

Contents lists available at ScienceDirect

Journal of Aerosol Science

journal homepage: www.elsevier.com/locate/jaerosci

Nozzleless spray cooling using surface acoustic waves

Kar M. Ang [a], Leslie Y. Yeo [b], James R. Friend [b], Yew M. Hung [a], Ming K. Tan [a,*]

[a] School of Engineering, Monash University Malaysia, 47500 Bandar Sunway, Selangor, Malaysia
[b] Micro/Nanophysics Research Laboratory, RMIT University, Melbourne, VIC 3001, Australia

ARTICLE INFO

Article history:
Received 9 August 2014
Received in revised form
12 October 2014
Accepted 12 October 2014
Available online 18 October 2014

Keywords:
Surface acoustic wave
Atomization
Nanoparticles
Spray cooling
Heat transfer

ABSTRACT

Surface acoustic wave (SAW) atomization is an attractive approach for generating monodispersed microdroplets for a diversity of applications, from drug delivery to mass spectrometry, due to its reliability, miniaturizability, and portability. Here, we demonstrate a nozzleless spray cooling technique based on SAW atomization, with the key advantage of downward scalability: increasing the operating frequency facilitates the fabrication of a chip-sized atomizer to use in compact cooling of electronic devices. Using deionised water, cooling is improved by 15% when the atomization rate is increased by 40%; when the gap separating the SAW device and heat source is halved, the cooling is improved by 20%. By constructing the device such that the atomized droplets are easily deposited upstream of the flow circulation, the performance is improved further. The atomization of CuO nanoparticle suspensions (at 3%) increased the cooling performance by 30%. Merely increasing the nanoparticle mass concentration in the suspension from 1% to 3% leads to an improvement in the cooling by 10% due to the deposition and formation of nanoparticle clusters on the heated surface, thereby increasing the total surface area. Further increases in the nanoparticle concentration to 10% however results in a diminution in the cooling due to the increase in the suspension viscosity μ, that leads to a reduction in the atomization rate $\dot{m} \sim \mu^{-1/2}$ for a given input power. Finally, we demonstrate the concept of using tapered finger transducers to selectively enhance local cooling in a desired area by simply changing the excitation frequency, without requiring repositioning of the SAW device.

1. Introduction

With the ever-increasing demand for high density electronic devices packed with millions to billions of transistors, and the associated heat generated during their operation, proper thermal management has long been important and is now a key driver of device design. This is because the performance and lifetime of these compact electronic devices, including microprocessors, laser diode arrays, X-ray anodes, light-emitting diodes (LED) and many others, are intrinsically limited by the cooling efficiency. For instance, Narendran & Gu (2005) reported that the life span of LEDs decreases exponentially with increasing temperature. Many different types of cooling techniques have been proposed to address these problems, handling extreme heat fluxes in confined spaces. Such techniques include (Agostini et al., 2007; Ebadian & Lin, 2011; Kim, 2007): single- and two-phase flow microchannel and porous media heat exchangers, thermosyphons, heat pipes, jet impingement cooling, and spray cooling.

* Corresponding author.
E-mail address: tan.ming.kwang@monash.edu (M.K. Tan).

http://dx.doi.org/10.1016/j.jaerosci.2014.10.004
0021-8502/

Among these techniques, spray cooling is one of the most promising due to its high heat-flux removal capability. Spray cooling involves the generation of fine droplets, which subsequently impinge on a heated surface (i.e., the heat source). The impinged droplets then either form a thin liquid film atop the heated surface which subsequently evaporates, or, evaporates immediately without formation of the thin film. Considering a small droplet at room temperature that deposits on a heated surface, the amount of heat required to vaporize the droplet consists of the sensible and latent heats, i.e.,

$$Q = m(c_p \Delta T + h_{fg}), \tag{1}$$

where m is the mass of the droplet, c_p is the specific heat at constant pressure, ΔT is the change in temperature from the droplet's initial condition to its saturation temperature, and h_{fg} is the latent heat of vaporization. Smaller droplets require less energy for vaporization and therefore vaporize at a faster rate than their larger counterparts, altogether leading to a faster rate of cooling as the droplet size is reduced.

Generally, nozzles are employed to deliver the spray in spray cooling techniques, and the diameter of the nozzles used define the droplet size. A piezoelectric transducer is frequently used as the actuator to pressurize the liquid in a chamber such that it is repeatedly forced through an orifice, forming individual droplets at high speed, resulting in the generation of many fine droplets that impinge on the heated surface (Hsieh et al., 2014; Lim et al., 2008). Another technique known as electrohydrodynamic atomization or electrospraying (Cloupeau & Prunet-Foch, 1994; Nguyen et al., 2014; Wang & Mamishev, 2012a,b; Wilhelm et al., 2003) employs an electric field as the droplet generation mechanism wherein counterions in the fluid are attracted to the tip of the meniscus protruding from a nozzle when it is raised to an applied potential. Due to Coulombic repulsion, the tip, which deforms into a conical shape known as the Taylor cone (Taylor, 1964), subsequently disintegrates to produce a thin jet that breaks up due to Coulombic fission or hydrodynamic instabilities to form the droplets (Sen et al., 2007), which are then attracted to the surface of the collection electrode, which acts as the thermal exchange surface. While electrospray cooling is able to achieve high heat removal rates, a disadvantage of the technique is the requirement of a very high DC voltage supply ($\sim 10^3$ V). Moreover, one of the limitations of nozzle-based devices is their propensity to clog, either by condensates or by vapor lock with gas entrapment in the orifice (Lohse et al., 2008). Clogging can also be caused by the hydrodynamic bridging (Lee et al., 2012; Ramachandran & Fogler, 1999), which occurs upon the arrival of several foreign particles or impurities at the nozzle simultaneously, forming particle bridges. The size of these foreign particles can be an order of magnitude smaller than the diameter of the nozzle. In a different study reported by Georgieva et al. (2010) on the microchannel flow of a solution suspended with nanoparticles, they found that hetero-coagulation of these suspended nanoparticles with the micron-sized impurities in the solutions can lead to flow induced aggregation and clogging; the diameter of impurities can be significantly smaller than the size of the channels. Due to the higher possibilities of clogging on nozzle-based devices, regular shutdown for cleaning and maintenance is required. In contrast, nozzleless devices employ a spatiotemporally varying, externally applied force to destabilize the free surface of the liquid, leading to its breakup into a mist of fine droplets whose size is a function mainly of the fluid's physical properties. In the remaining portion of this paper, nozzleless spray cooling using surface acoustic waves is shown to be an effective technique to generate a plume of microdroplets for cooling.

In this study, we demonstrate a spray cooling technique that employs surface acoustic wave (SAW) atomization as the spray droplet generation mechanism. The SAW device consists of an interdigital transducer (IDT) patterned on a piezoelectric substrate, which, upon application of a sinusoidal electrical wave, generates a mechanical wave that is mostly confined adjacent to the surface of the substrate, i.e., within one acoustic wavelength from the surface. Upon contact with a fluid placed atop the substrate, the leakage of acoustic radiation into the fluid generates sound that propagates into the fluid responsible for both an acoustic radiation pressure at the free surface of the liquid and a bulk momentum transport in the liquid known as acoustic streaming (Ding et al., 2013; Friend & Yeo, 2011). Consequently, different phenomena—vibration (Miyamoto et al., 2002), transport (Tan et al., 2007), mixing (Shilton et al., 2008, 2014), and jetting (Guo et al., 2014; Tan et al., 2009)—can be induced within the liquid body depending on the magnitude of the surface acceleration on the substrate, itself controlled by the amount of input power delivered to the device. Beyond a critical power or substrate acceleration, however, these phenomena are subsumed by the breakup of the free surface of the liquid as it atomizes to produce a mist of aerosol droplets, approximately 1–10 μm in diameter, typically ejected at velocities up to 1 m/s (Chono et al., 2004; Collins et al., 2012; Qi et al., 2008, 2009). The focus of this work is to harness this ability to produce a high-velocity stream of atomized droplets to reduce the surface temperature of a heated plate placed at a certain separation distance, h_{gap}, from the substrate as a means for efficient nozzleless spray cooling. A major advantage of the technique is the ease with which the SAW devices can be miniaturized for portable applications, an important consideration in future electronic chip cooling applications. A brief comparison of the important characteristics between the nozzle-less spray using SAW device and the nozzle-based spray using piezoelectric transducer and electrospray is shown in Table 1.

2. Experiments

Figure 1(a) illustrates the focusing single-phase unidirectional transducers (Fig. 3(a)) used in the experiments, fabricated on a 128° rotated *Y*-cut *X*-propagating, single-crystal lithium niobate ($LiNbO_3$) piezoelectric substrate. A sinusoidal electric signal generated from a function generator (WF1966, NF Corporation, Japan) was amplified using a high frequency amplifier (25A250A, Amplifier Research, USA), and subsequently applied to the IDT to generate a SAW that propagates on the substrate. The frequency of the signal was set to match the resonant frequency f_{SAW} of the device, set by the gap and spacing

Table 1
A brief comparison of different techniques to generate droplets for cooling of micro-devices.

Technique to generate droplets	Fluid	Flow rate (ml/min)	Droplet size (μm)
Nozzleless: SAW atomization (Qi et al., 2008)	Water	0.5–0.7	1–10
Nozzle-based: piezoelectric actuator (Huang et al., 2005)	Water	0.5–1.2	20–80
Nozzle-based: electrospray (Deng & Gomez, 2011)	Ethanol	0.4–1.7	5–30
Nozzle-based: piezoelectric micropump (Hsieh et al., 2014)	Water	2.4–32	7–35

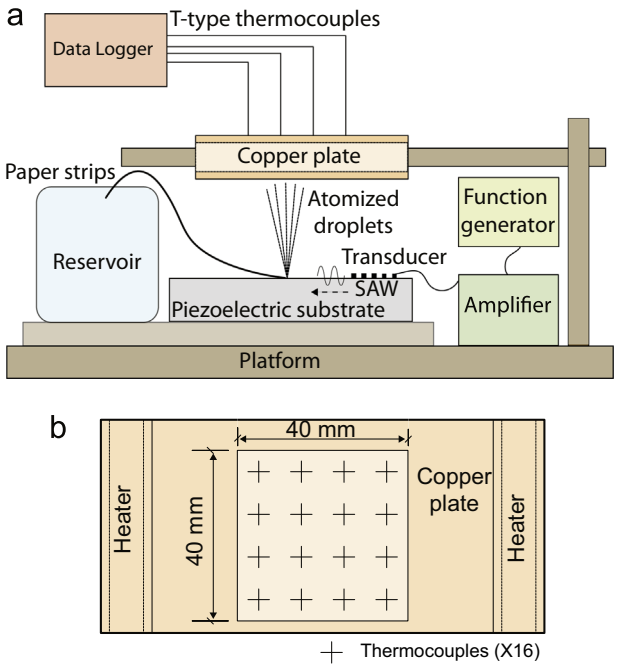

Fig. 1. (a) Sketch illustrating the experimental setup (not to scale). (b) Top view of the copper plate, within which two resistance heaters of cylindrical shape are embedded. A total of 16 thermocouples were placed in a two-dimensional array to map the temperature profile of the study area. The thermocouples were connected to a data logger in order to record the fluctuation in the temperature at a sampling rate of 1 Hz.

of the IDT structure. Cleanroom paper (porous media) (WIP-100DLE, SUOREC, Malaysia) was used to deliver deionised (DI) water from a beaker to the surface of the substrate through capillary action, forming a thin liquid film on the substrate at the edge of the paper strip from which the atomization occurs, as depicted in Fig. 2. Two layers of paper strips were used as a wick to ensure sufficient water flow to the SAW device, preventing depriming of the wicking material and failure of the atomization. To drive continuous atomization at lower power, the input signal was amplitude modulated at f_m (Rajapaksa et al., 2014). The measured total input power to the SAW device was in the range of 1.0–2.5 W.

To investigate the cooling effectiveness of the microdroplets atomized by the SAW, a 500 μm thick copper plate was embedded with two cylindrical resistance heaters; the heaters were tightly inserted into pre-drilled cylindrical holes to ensure effective heat transfer from the heaters to the copper plate. The plate was then placed directly above the SAW device and 16 thermocouples were distributed on the surface of the plate (4 cm × 4 cm) to map its temperature profile (see Fig. 1 (b)). The resistance heaters were connected in parallel and powered by a DC voltage power supply. For each experiment, the instantaneous temperature was recorded at a sampling rate of 1 Hz. The experiments were conducted in an enclosed chamber in which the ambient temperature was maintained at 26.5 °C to ensure that the results were not affected by the ambient conditions. Once the heated plate reached its initial steady-state temperature, both the temperature recording and the SAW atomization were initiated. Each measurement was terminated once the final steady-state temperature was reached, generally achieved in less than ten minutes.

A cooling enhancement ratio (CER) is employed to quantify the improvement in cooling in the presence of microdroplets generated by SAWs. From Newton's law of cooling

$$\dot{Q} = hA(T_s - T_\infty), \tag{2}$$

in which $\dot{Q}$ is the heat transfer rate, the convective heat transfer coefficient can be expressed as $h = q''/(T_s - T_\infty)$, where $q'' = \dot{Q}/A$ is the heat flux, T_s is the surface temperature of the plate and T_∞ is the ambient temperature. The heat flux can be approximated as $q'' = VI/A$, where V is the applied voltage, I is the current, and A is the surface area of the heater. The cooling

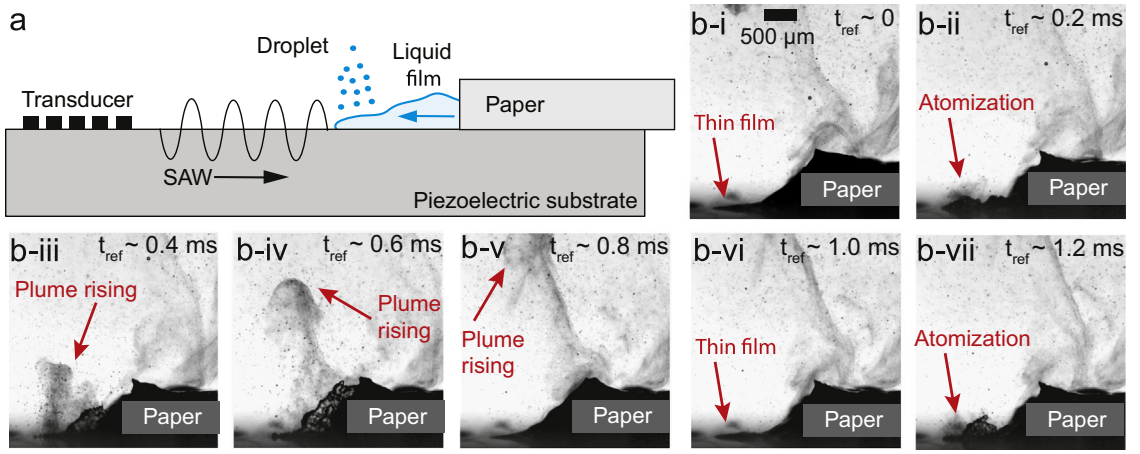

Fig. 2. (a) Schematic illustration of the SAW atomization process from a thin fluid meniscus that forms at the edge of the paper strip. Note that while the SAW is traveling from left-to-right, the liquid thin film spreads from right to left (Rezk et al., 2012); the sketch is not to scale. (b) Sequential experimental images showing atomization using $f_{SAW} = 29.5$ MHz SAW amplitude modulated at $f_m = 1000$ Hz: (i) formation of the thin liquid film at the tip of the paper strip, (ii) onset of atomization in which the film breaks up to form, (iii–v) a plume of tiny droplets that are ejected upward away from the device. (vi) and (vii) The process is repeated as fluid is drawn from the paper by the SAW to maintain the thin fluid meniscus as it atomizes. Based on the images recorded at 10,000 frames per second, one complete process takes approximately 1 ms (i.e., 1 kHz), which is identical to the modulation frequency.

enhancement ratio is then defined as the ratio of the heat transfer coefficient when cooling is aided by the SAW, h_{SAW}, to the coefficient in the absence of SAW cooling, h_0, i.e., $CER = h_{SAW}/h_0$. Since the power input to the heater is kept constant in each experiment, i.e., q'' is constant, it then follows that

$$CER \equiv \frac{h_{SAW}}{h_0} = \frac{T_0 - T_{0,\infty}}{T_{SAW} - T_{SAW,\infty}}, \tag{3}$$

where T_0 is the steady-state temperature of the plate and $T_{0,\infty}$ is the ambient temperature in the absence of SAW cooling, whereas T_{SAW} and $T_{SAW,\infty}$ are their counterparts when SAW cooling is applied. The performance of the SAW cooling can therefore be evaluated from the CER: the larger its value, the more effective the cooling. In the sections to follow, we examine (i) the effectiveness in the cooling with the SAW microdroplets, (ii) further cooling enhancement through the use of nanoparticle suspensions, and (iii) the possibility of targeted local cooling with the use of a tapered IDT.

2.1. Cooling enhancement with SAW atomized microdroplets

To study the basic parameters that underpin the nozzleless spray cooling process using SAW atomization, we employ deionised water as the test fluid given its high thermal capacity and atomization ease via SAW. We first explore variations in the atomization rate $\dot{m}$—achieved here by altering the amplitude modulation frequency (within the range $f_m = 1$–15 kHz)—which we expect to have a direct impact on the cooling rate given higher deposition rates of the droplets on the surface with increases in the atomization rate. In addition, we explore the effect of different initial surface temperatures of the heated plate T_s by varying the input power to the heaters, the effect of the separation distance between the SAW device and the heated surface H_{gap} (since it is expected that the deposition of the atomized droplets depends on this parameter), and the position of the SAW device. The latter aspect is examined since the heated surface can give rise to airflow circulation adjacent to the surface due to natural convection; it is then possible to maximize droplet deposition on the surface through strategic positioning of the SAW device with respect to the convective flow.

2.2. Cooling enhancement with SAW atomized nanoparticle suspensions

There have been a number of studies to date reporting significant improvement in heat transfer through the addition of sub-100-nm particles to the coolant (Fedele et al., 2012; Heris et al., 2006; Özerinç et al., 2010), the thermal conductivity and convective heat transfer coefficient increasing significantly with an increase in the nanoparticle concentration. Nanoparticle suspensions replaced the DI water as the atomization fluid with five different weight ratios—1%, 2%, 3%, 5% and 10%—of copper (II) oxide (CuO) nanoparticles (Sigma-Aldrich, Malaysia) with diameters below 100 nm in deionised water were prepared by ultrasonication (Q700, Qsonica, Newton, USA). The viscosity μ and the surface tension γ of the suspensions were characterized prior to each experiment, in which the suspension of known concentration was drawn through the paper strips onto the SAW substrate and subsequently atomized when the input power to the device was applied. Microscopic images of the surface of the heated plate were then examined to quantify the deposition rate of the nanoparticles on its surface; briefly, the images were rendered in grayscale and the pixel intensities were analyzed using MATLAB (MathWorks Inc., USA). In addition to using prepared nanoparticle suspensions, we also examined the possibility of using the SAW to

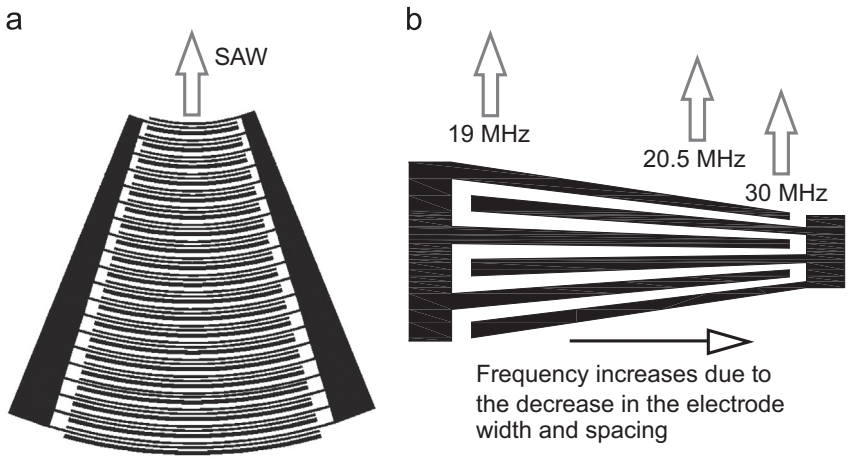

Fig. 3. Types of IDTs used in the experiments (not to scale). (a) Focusing single-phase unidirectional transducer (SPUDT) with resonant frequency 29.5 MHz. (b) Tapered transducer with a resonant frequency band between 19 and 30 MHz.

disperse the raw, agglomerated nanoparticles as supplied in solution, eliminating the labor-intensive and expensive ultrasonication process. In this case, a known quantity of nanoparticles in dry powder form was first deposited on the SAW substrate immediately adjacent to the channel outlet defined by the edges of the paper strips. On activating the SAW, the working fluid was then drawn out from the paper strips, drawing up and dispersing the nanoparticles in the solution prior to atomization—hence circumventing difficulties due to a reduction in the heat transfer rate as a consequence of particle agglomeration and sedimentation.

2.3. Tapered transducers

The final part of the study involved a demonstration of the concept of locally targeted cooling at specific locations along a single spatial dimension through the use of the tapered IDT structure (Wu & Chang, 2005) which possesses a linear change width and spacing along the IDT's width, as depicted in Fig. 3(b) and in place of the focused IDTs of the previous experiments. In contrast to the generation of SAWs with a single frequency (here, $f_{SAW} = 29.5$ MHz) using the focused IDT structure (Fig. 3(a)), tapered IDTs possess a broad frequency band (here, the f_{SAW} band ranges between 19 and 30 MHz). By using different operating frequencies for the signal input to the IDTs, it is then possible to confine the propagation of the SAW to a local region corresponding to the location where the applied frequency is equal to the resonant frequency specified by the width and the gap of the transducer at that location; the width of the SAW that is generated is approximately commensurate with the SAW wavelength—of 100 μm order. This ability to choose the specific location of the SAW and hence the position from which atomization ensues, with 100 μm order precision and simply by varying the excitation frequency, offers a powerful means to rapidly and locally target a specific location for enhanced cooling. We note that this is however achieved with a reduction in the atomizer efficiency; unlike the unidirectional SPUDT, the SAW generated using the tapered IDTs is bidirectional, generating SAWs that travel both in the forward and backward directions. In this case of the tapered IDTs, the modulation frequency f_m is fixed at 1 kHz.

3. Results and discussion

3.1. Cooling enhancement with SAW atomized microdroplets

3.1.1. Atomization rate

Figure 4(a) reports the CER at different atomization rates, controlled by altering the modulation frequency f_m while maintaining the same initial temperature of 101 °C across the experiments: atomization rates of 44.03, 37.17, 32.69 and 29.03 ml/h were obtained with $f_m = 1$, 5, 10, and 15 kHz, respectively, from which we observe a corresponding linear response in the mean CER values of 1.34, 1.25, 1.21 and 1.16. The relation CER $\sim \dot{m}$ then implies that $h_{SAW} \sim \dot{m}$ from Eq. (3). Recalling the heat required to vaporize a droplet from Eq. (1), the total heat removal rate from the heated surface as a consequence of all droplets deposited on the surface is then

$$\sum \dot{Q} = \dot{m}(c_p \Delta T + h_{fg}), \tag{4}$$

assuming that all droplets generated through the SAW atomization reach the surface. If it can be further assumed that the cooling is predominately due to the presence of the microdroplets, combining Eqs. (2) and (4) then yields the linear $h_{SAW} \sim \dot{m}$ relationship observed in Fig. 4(a). Extrapolating the relationship, we expect the cooling efficiency to gradually decrease to approach the limit based on natural convection as the atomization rate reduces to less than 15 ml/h.

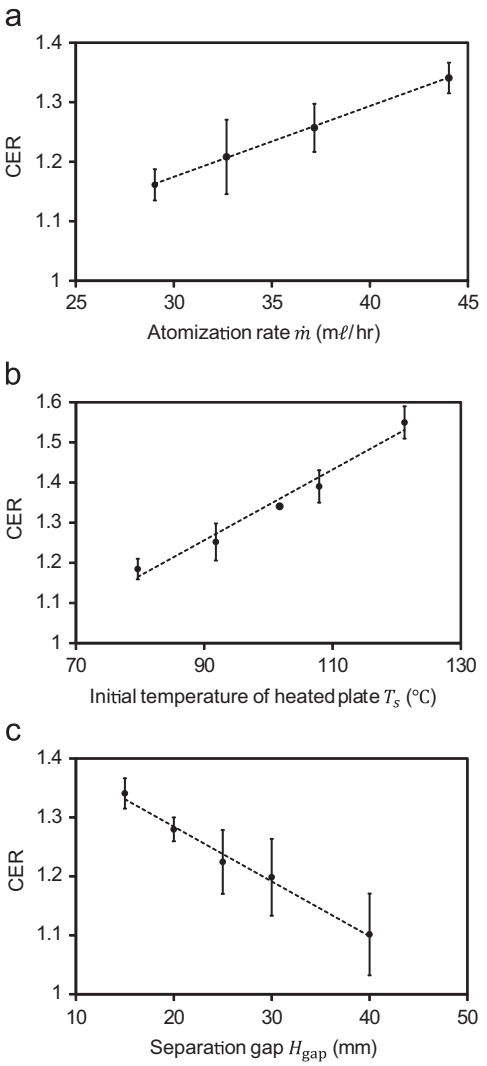

Fig. 4. Cooling enhancement ratio CER as a function of (a) the atomization rate $\dot{m}$, (b) the initial surface temperature of the heated plate T_s, and, (c) the separation gap H_{gap}. Error bars indicate a ± 2 standard deviation (95% confidence level) from the mean. The trend lines were added to aid visualization.

3.1.2. *Initial surface temperature of the heated plate*

Figure 4(b) indicates the enhancement in the cooling as reflected by the increase in CER values as the initial surface temperatures of the heated plate T_s are increased, achieved by increasing the input power to the heater while maintaining the same atomization rate by keeping the modulation frequency constant at 1 kHz. Given that the ambient temperature T_∞ is held constant, the increase in T_s corresponds to an increase in the temperature difference $T_s - T_\infty$, thus suggesting that CER $\sim T_s$. Assuming that $\dot{Q}$ and A constant, Eq. (2) however yields $h \sim 1/(T_s - T_\infty)$, therefore suggesting that larger values of T_s and hence the temperature difference lead to a reduction in h and hence a lower cooling rate. Nevertheless, we note that the heat transfer coefficient in the absence of the microdroplets h_0 reduces at faster rate than the same coefficient when microdroplets are employed h_{SAW}, underwriting the increasing CER values for higher surface temperatures T_s. We also note from extrapolating the result in Fig. 4(b) that the use of microdroplets to enhance cooling is no longer effective when the surface temperature of the heated plate drops below approximately 60 °C.

3.1.3. *Separation gap*

We next explored the effect of five different gaps, 1.5, 2, 2.5, 3 and 4 cm, on the cooling enhancement that can be obtained with the SAW; here, both modulation frequency and the initial temperature of the heated plate were maintained at 1 kHz and 101 °C, respectively. Figure 4(c) shows an inversely proportional relationship between the CER and the separation distance, i.e., CER $\sim H_{gap}^{-1}$. The drop in the cooling enhancement due to increasing separation distance can be attributed to an increasing proportion of droplets failing to deposit on the surface of the heated plate. While the droplets are ejected at velocities on the order of 1 m/s (Qi et al., 2008) due to the high substrate acceleration on the order of 10^7 m/s^2 as the SAW

traverses it; the air drag typically retards the droplet momentum in-flight such that an increasingly large number of droplets fail to reach the surface as the separation distance increases. Therefore, the atomized droplet is experiencing a deceleration while moving from the surface of the SAW device to the surface of the copper plate. For a simple linear motion of a droplet, one can express the motion using the following relationship:

$$u_2^2 = u_1^2 - 2a_p(x_2 - x_1), \tag{5}$$

where u_2 is the droplet velocity adjacent to the SAW, u_1 is the droplet velocity adjacent to the copper plate, a_p is the deceleration of the droplet, and $x_2 - x_1 \approx H_{gap}/\cos\theta_R$ is the distance traveled by the droplet, $\theta_R = \sin^{-1}(c_f/c_{SAW}) \approx 22^\circ$ is the *Rayleigh angle*, $c_f \approx 1490$ m/s is the sound speed in the liquid and $c_{SAW} \approx 3990$ m/s is the sound speed in the substrate. Re-arranging Eq. (5) gives

$$a_p = \left(\frac{\cos\theta_R}{2}\right)\frac{u_1^2 - u_2^2}{H_{gap}}. \tag{6}$$

The equation above shows that the deceleration of the droplet is inversely proportional to the separation gap, i.e., $a_p \sim H_{gap}^{-1}$, indicating the reduction in inertial force—$F_I \sim m_p a_p$, where m_p is the mass of the droplet—as the droplet travels from the SAW device to the copper plate. In any case, extrapolation of the result in Fig. 4(c) again shows that the use of droplets to enhance cooling becomes negligible beyond a separation gap of 50 mm.

3.1.4. Position of the SAW device

When the surface temperature is higher than the ambient temperature, natural convection arising from the difference in the air density produces a convection current and hence circulation flow adjacent to the plate. Close to the surface of the heated plate, the droplet is therefore subjected to an additional drag due to this natural convection current, estimated to be on the order of $F_D \sim \mu_a R_p u_p \sim 10^{-10}$–$10^{-11}$ N, where $\mu_a \sim 10^{-5}$ kg/ms is the air viscosity, $R_p \sim 10^{-5}$–10^{-6} m is the droplet radius and $u_p \sim 1$ m/s its velocity. At separation distances when the droplet momentum is retarded sufficiently such that it is comparable to the order of magnitude of this convective drag, i.e., when $H_{gap} \sim 40$ mm, it is possible that the droplets can be seeded upstream of the circulation through judicious positioning of the SAW devices and hence the position of the atomization plume such that the droplets are transported by the flow to the surface of the plate. This effect can be seen in Fig. 5(a) wherein the device was positioned such that the atomized plume directed the droplets upstream of the circulation

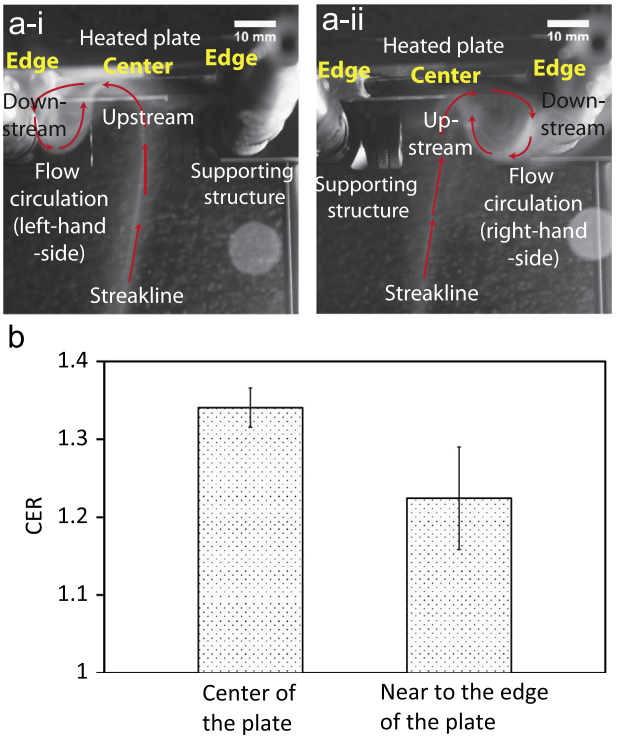

Fig. 5. (a) Flow circulation cell adjacent to the heated plate surface generated due to natural convective currents, visualized through streaklines obtained through injection of smoke particles. Positioning of the SAW device and hence the atomization plume allowed droplets to be seeded upstream of the flow circulation (center of the heated plate) such that they are directed towards the surface of the plate; (i) stronger circulation on the left-hand-side, and (ii) stronger circulation on the right-hand-side of the heated plate. (b) Corresponding CER values for both cases. Error bars indicate a ± 2 standard deviation (95% confidence level) from the mean. A Student's *t*-test indicates that the difference in the CER values for both cases are statistically significant given $p = 0.019 < 0.05$.

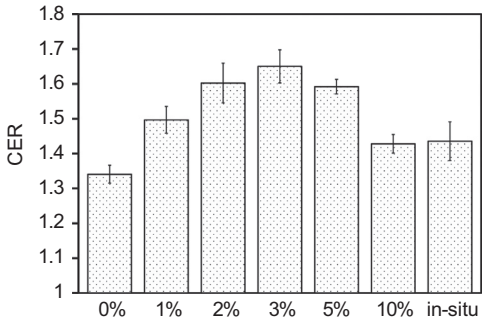

Fig. 6. Cooling enhancement ratio for prepared nanoparticle suspensions with different nanoparticle mass concentrations: 1%, 2%, 3%, 5% and 10%. Also shown are the results obtained for the raw, agglomerated nanoparticle suspension processed as-provided using the SAW ($\approx 1.7\%$ mass concentration) and DI water without nanoparticles (0% mass concentration). Error bars indicate ± 2 standard deviation (95% confidence level) from the mean. Student's *t*-test (Table 2) suggests that the increase in the CER value from a 1% concentration suspension to a 3% concentration suspension is statistically significant ($p < 0.05$). Similarly, the decrease in the CER as the suspension concentration is increased from 3% to 10% is also statistically significant ($p < 0.05$).

Table 2
Probability values from Student's *t*-test used to assess the significance of varying the nanoparticle suspension concentration on the CER. $p < 0.05$ denotes statistical significance.

	1%	2%	3%	5%	10%	in situ
0%	0.001	0.003	0.005	0.0	0.002	0.002
1%	–	0.007	0.021	0.003	0.008	0.030
2%		–	0.149	0.534	0.007	0.003
3%			–	0.112	0.009	0.003
5%				–	0.0	0.008
10%					–	0.641

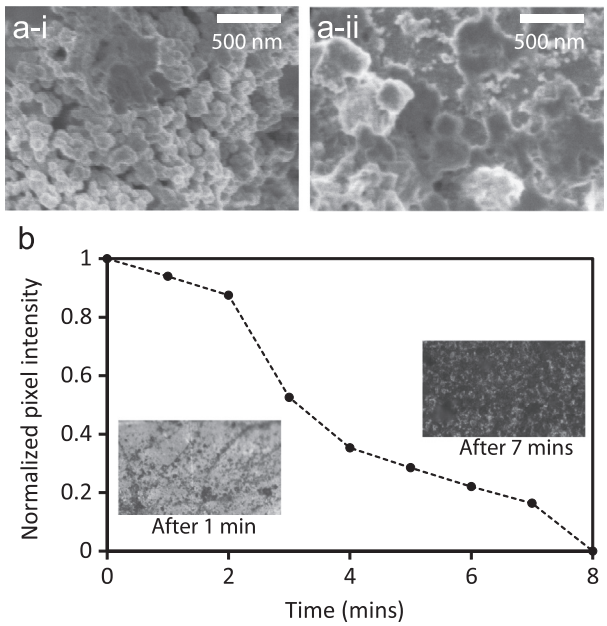

Fig. 7. (a) Scanning electron microscopy (SEM) images showing (i) the powder of nanoparticles with diameter less than 100 nm prior to atomization and deposition, and (ii) the deposited nanoparticles on the heated plate. (b) Time-dependent normalized mean pixel intensity I_p of the captured SEM images as a measure of the nanoparticle coverage on the heated surface over time during the atomization: $I_p = 1$ refers to a bare surface without the presence of nanoparticles and $I_p = 0$ refers to a surface completely covered with the nanoparticles. The dotted line was added to aid visualization. The insets show images of the nanoparticles deposited on the heated surface after 1 and 7 min of spray via SAW atomization; the images were captured using optical microscope with a $\times 50$ magnification.

whose trajectory was visualized using smoke particles, leading to increased droplet deposition on the surface and hence an improvement in the CER (Fig. 5(b)). Conversely, targeting the atomized droplets at the downstream end of the flow led to a diversion of the droplets away from the surface of the plate, resulting in reduced CER values (Fig. 5(b)).

3.2. Cooling via SAW generated microdroplets with suspension of nanoparticles

CER values for different nanoparticle concentrations are given in Fig. 6 and Table 2 for constant modulation frequency (1 kHz), initial plate surface temperature (101 °C) and separation distance (15 mm). We observe that an optimum suspension mass concentration around 3% exists, where a CER value approximately 30% higher than that in the absence of nanoparticles (i.e., DI water alone) was obtained. We thus note that cooling is enhanced initially as the nanoparticle concentration is increased, consistent with that in previous studies (Fedele et al., 2012; Heris et al., 2006). This can be attributed to a nanoparticle layer covering the surface of the heated plate when atomized nanoparticle-laden droplets deposit on the surface and the liquid evaporates. Figure 7(a) shows images captured using field-emission scanning-electron-microscopy (Hitachi SU8010) of (i) the raw nanoparticle powder with diameter below 100 nm and (ii) the nanoparticle deposited on the heated surface after atomizing for 8 min; it can be seen that the deposited nanoparticles agglomerated to form clusters of different sizes with typical 1 μm order length scales. Figure 7(b), reporting the normalized mean pixel intensity I_p of the captured images as a function of time and quantifying the particle deposition and associated surface coverage, shows an increase in the nanoparticle density. The nanoparticle clusters then result in an increase in the surface area for heat transfer, therefore leading to an enhancement in the cooling, consistent with the findings reported by

Table 3
Physical properties of the nanoparticle suspension in DI water as a function of the mass concentration. Δ_{max} represents the percentage difference of the physical property when the suspension concentration is varied between 1% and 10%. The last column tabulates the relative change in the atomized droplet diameter as the property is varied; D_{Ref} refers to the reference diameter.

Concentr. (%)	ρ (kg/m^3)	γ (N/m)	μ (Ps s)	
1	1008	0.205	0.000788	D_{Ref}
2	1017	0.219	0.000814	$D \sim D_{Ref}$
3	1026	0.236	0.000772	$D \sim D_{Ref}$
5	1044	0.263	0.001114	$D \sim 0.8D_{Ref}$
10	1092	0.312	0.001976	$D \sim 0.5D_{Ref}$
Δ_{max}	8%	51%	150%	

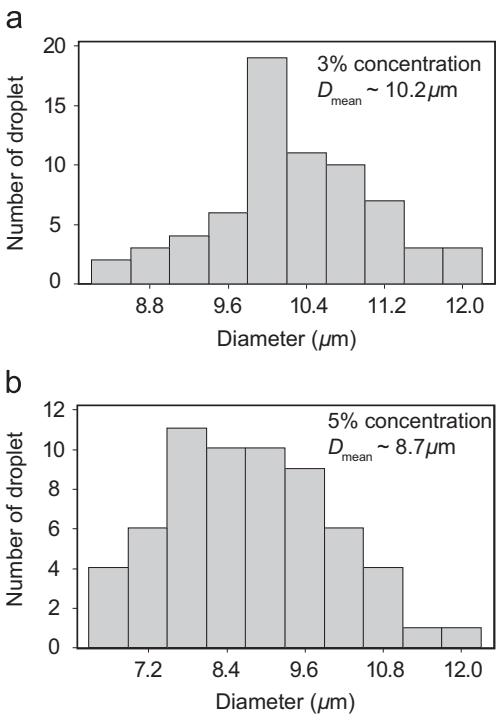

Fig. 8. Size distribution of the atomized droplets from solutions of (a) 3% and (b) 5% of nanoparticle concentration.

Zhang et al. (2014) who found an improvement in the heat transfer for a spray cooled microstructured surface containing 10 μm features compared to smooth surfaces.

Beyond the optimum nanoparticle concentration, however, there is an observed decrease in the cooling efficiency with further increases in the nanoparticle concentration. This can be attributed mainly to a change in the fluid properties—density ρ, viscosity μ, and coefficient of surface tension γ—with the increasing nanoparticle concentration (see Table 3). While both density and surface tension appear to increase linearly with the nanoparticle concentration, consistent with reported findings (Khaleduzzaman et al., 2013) and therefore playing a relatively insignificant role, the increase in the suspension viscosity appears, on the other hand, to be nonlinear and becomes increasingly significant above a concentration of 3%—again consistent with reported findings (Fedele et al., 2012; Zhu et al., 2010). Such an increase in the viscosity could lead to a considerable change in the atomized droplet size, which scales as $D_p \sim \gamma^{1/3}\rho^{2/3}/\mu$ (Collins et al., 2012). For constant SAW frequency f_{SAW} and substrate surface displacement amplitude ξ_0 (a measure of the input power to the SAW device), the relative change in the droplet diameter as a function of the change in the nanoparticle suspension concentration is given in the last column in Table 3. This indicates the change in the atomized droplet diameter and hence its effect on the cooling enhancement is insignificant for nanoparticle concentrations below 3%, but becomes increasingly significant beyond this optimum concentration. To verify the relative change in the droplet diameter for solutions with different nanoparticle concentrations, as shown in Table 3, two solutions with 3% and 5% of nanoparticle concentration were atomized and the process was captured using a high speed camera (M310, Phantom, New Jersey, USA) equipped with a magnifying lens (1-50486, Navitar, Rochester, USA). The droplet size is estimated using the recorded images. For the solution with 3% nanoparticle concentration, the side distribution (95% confidence interval) is within 10.0–10.4 μm (see Fig. 8(a)) and the mean diameter is 10.2 μm, whereas for the solution with 5% nanoparticle concentration, the size distribution (95% confidence interval) is within 8.4–9.1 μm (see Fig. 8(b)) and the mean diameter is 8.7 μm. Therefore, the relative change in the droplet diameter for the solutions with 3% and 5% nanoparticle concentration is $D_{3\%} \sim 0.85D_{5\%}$, which is very close to the predicted result $D_{3\%} \sim 0.8D_{5\%}$ (see Table 3).

For a constant atomization rate, however, we expect the cooling to improve with decreasing droplet dimension with increasing nanoparticle concentration beyond 3%. That the contrary is observed therefore suggests that the rate of atomization varies as the nanoparticle concentration is increased. We thus examine the atomization rate as a function of the fluid physical properties by defining two dimensionless parameters, noting the importance of the thickness of the film emanating from the edge of the paper strip H_f (Fig. 2) on the atomization process that was elucidated in previous atomization studies (Collins et al., 2012; Qi et al., 2008): $[\gamma/(\rho H_f c_f^2)]^{1/2}$ and δ_v/H_f, where c_f is the sound speed in the liquid and $\delta_v \equiv [\mu/(\rho f_{SAW})]^{1/2}$ is the viscous boundary layer thickness (Friend & Yeo, 2011). The former represents the inverse of the film Weber number, i.e., $We_f \sim \rho H_f c_f^2/\gamma$, capturing the ratio of the destabilizing acoustic inertial force to the stabilizing capillary force acting on the thin film. The latter represents the relative distance over which viscous absorption of the substrate oscillation influences the flow in the liquid film. The dependence of the atomization rate on these parameters is demonstrated in Fig. 9, in which we find that $\dot{m} \sim (\rho H_f c_f^2/\gamma)^{1/2}(H_f/\delta_v)$, from which we note the expected inverse dependence on the atomization rate with the surface tension $\dot{m} \sim \gamma^{-1/2}$ and viscosity $\dot{m} \sim \mu^{-1/2}$—not unexpected given the increasing difficulty in destabilizing the free surface with larger restoring capillary stresses and increasing viscous dissipation, the latter due to a decrease in the inertial energy available to destabilize the free surface. The reduction in the CER with increasing nanoparticle concentration beyond 3% in Fig. 6 can then be predominantly attributed to the suppression of the atomization as a consequence of these factors. Interestingly, the above also suggests that the excitation frequency f_{SAW} needs to be increased to maintain the thickness of viscous boundary layer δ_v if the atomization rate is to be maintained at higher nanoparticle concentrations ($> 5\%$).

Sedimentation of the nanoparticles was nevertheless observed prior to atomization with the ultrasonically prepared nanoparticle suspensions, resulting in changes in the concentration of the suspensions that were atomized. To minimis this, and hence its effect on the atomized droplet diameter and the cooling enhancement, we experimented with *in situ* dispersion and atomization of the nanoparticles through the paper strip (see Section 2.2). Figure 6 reports the CER values

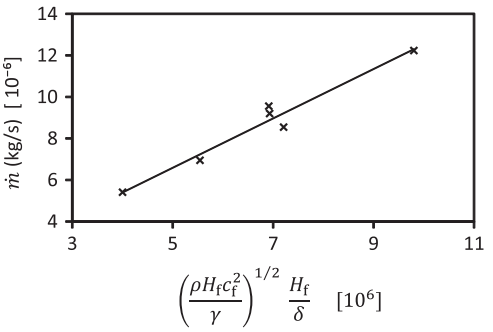

Fig. 9. Relationship between the atomization rate $\dot{m}$ and the dimensionless parameters representing the film Weber number $We_f \sim \rho H_f c_f^2/\gamma$ and the absorption depth ratio, δ_v/H_f. The solid line represents a least square fit ($R^2 = 0.96$) of the data and suggests that $\dot{m} \sim \rho(\gamma\mu)^{-1/2}$.

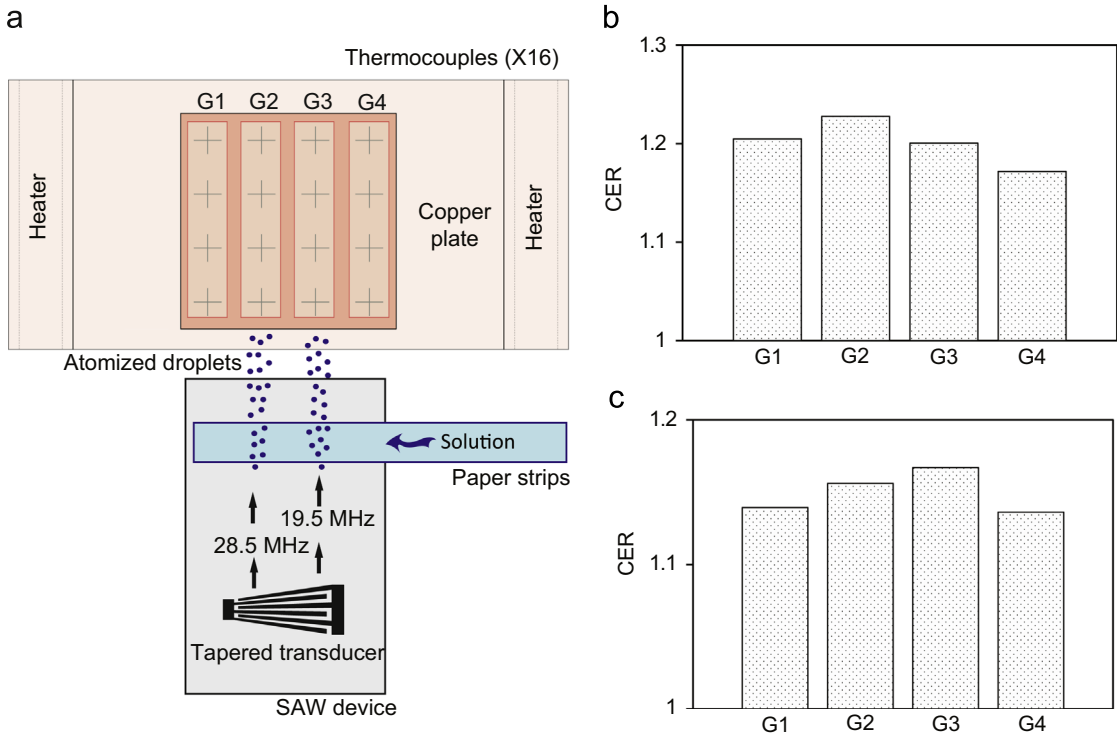

Fig. 10. (a) The positioning and grouping of thermocouples used to measure temperatures across the heated plate (not to scale). Within each group, the measured CER values when the excitation frequency was (b) 28.5 MHz and (c) 19.5 MHz were averaged over four measurements.

obtained with this process using a nanoparticle concentration of approximately 1.7%, showing it to be 10% higher than DI water lacking nanoparticles but inferior to prepared 1% concentration nanoparticle suspensions. Despite the greater nanoparticle concentration, the results were inferior, indicating the *in situ* deagglomeration was insufficient compared to the prepared nanoparticle solutions. This is likely due to the fact the deagglomeration occurs over at most a matter of minutes *in situ* but for hours with the prepared solutions.

3.3. *Targeting cooling via slanted finger transducer*

Given the demonstration of enhancing spray cooling with the SAW atomization, we now turn to briefly explore the possibility of local targeted cooling with the use of the tapered IDTs shown in Fig. 3(b). To provide evidence of localization without requiring repositioning of the SAW device, the 16 thermocouples were arranged into four groups depending on their location such that excitation of the IDT at two different resonant frequencies, 19.5 and 28.5 MHz, resulted in the generation of SAW aligned with groups G3 and G2, respectively, as illustrated in Fig. 10(a). With all other parameters held constant, Fig. 10(b) and (c) indicates elevated values of the CER at G3 and at G2 when the excitation frequency is 19.5 and 28.5 MHz, respectively, providing evidence that targeted local cooling can be achieved by simply varying the excitation frequency of the signal supplied to the SAW device. In addition, the method also allows simultaneous cooling of a few locations by exciting the tapered transducer at the desired frequencies.

4. Conclusions

Efficient cooling is crucial to electronic devices of this era and the next, an issue that needs to be addressed if further development of high performance microelectronic devices is to be achieved. In this work, we propose and demonstrate the concept of rapid cooling via SAW atomization. The technique is similar to spray cooling, but uses SAW atomization instead to generate the microdroplets, a major advantage being both the removal of the need for nozzles which are prone to clogging and hence declining performance, and the ease of scaling down the device, therefore making them appropriate for use in next generation electronic devices. In particular, our preliminary experimental results show that the cooling can be optimized by increasing the atomization rate while reducing the separation distance between the SAW device and the heat source. Judicious choice of the SAW device and hence the location of the atomization plume also allows one to exploit the natural convective current that arises such that the atomized droplets can be deposited at specific locations on the surface to be cooled. Further enhancement in the cooling was achieved by employing a nanoparticle suspension instead of a pure fluid,

wherein the cooling enhancement ratio was observed to increase with higher nanoparticle concentrations up to an optimum value beyond which a marked increase in the suspension viscosity resulted in different atomization rates and hence droplet sizes that led to a deterioration in the cooling performance. Finally, the use of tapered IDTs which operate over a range of resonant frequencies and shift the location of the propagating SAW across the substrate as a consequence, altogether within a single transducer structure, was shown to enable local targeting of the cooling without repositioning the SAW device, a very desirable feature for modern electronic devices.

Acknowledgments

The authors gratefully acknowledge funding for this work from the Fundamental Research Grant Scheme, Ministry of Higher Education Malaysia, through Project Grant no. FRGS/1/2013/SG02/MUSM/02/2 and financial support from the Green Electronics, Advanced Engineering Platform, Monash University Malaysia.

References

Agostini, B., Fabbri, M., Park, J.E., Wojtan, L., Thome, J.R., & Michel, B. (2007). State of the art of high heat flux cooling technologies. *Heat Transfer Engineering*, *24*, 258–281.
Chono, K., Shimizu, N., Matsui, Y., Kondoh, J., & Shiokawa, S. (2004). Development of novel atomization system based on saw streaming. *Japanese Journal of Applied Physics*, *43*, 2987.
Cloupeau, M., & Prunet-Foch, B. (1994). Electrohydrodynamic spraying functioning modes: A critical review. *Journal of Aerosol Science*, *25*, 1021–1036.
Collins, D.J., Manor, O., Winkler, A., Schmidt, H., Friend, J.R., & Yeo, L.Y. (2012). Atomization off thin water films generated by high-frequency substrate wave vibrations. *Physical Review E*, *86*, 056312.
Deng, W., & Gomez, A. (2011). Electrospray cooling for microelectronics. *International Journal of Heat and Mass Transfer*, *54*, 2270–2275.
Ding, X., Li, P., Lin, S.-C.S., Stratton, Z.S., Nama, N., Guo, F., Slotcavage, D., Mao, X., Shi, J., Costanzo, F., & Huang, T.J. (2013). Surface acoustic wave microfluidics. *Lab on a Chip*, *13*, 3626–3649.
Ebadian, M.A., & Lin, C.X. (2011). A review of high-heat-flux heat removal technologies. *Journal of Heat Transfer*, *133*, 110801.
Fedele, L., Colla, L., & Bobbo, S. (2012). Viscosity and thermal conductivity measurements of water-based nanofluids containing titanium oxide nanoparticles. *International Journal of Refrigeration*, *35*, 1359–1366.
Friend, J., & Yeo, L.Y. (2011). Microscale acoustofluidics: Microfluidics driven via acoustics and ultrasonics. *Review of Modern Physics*, *83*, 647–704.
Georgieva, K., Dijkstra, D., Fricke, H., & Willenbacher, N. (2010). Clogging of microchannels by nano-particles due to hetero-coagulation in elongational flow. *Journal of Colloid and Interface Science*, *352*, 265–277.
Guo, Y.J., Lv, H.B., Li, Y.F., He, X.L., Zhou, J., Luo, J.K., Zu, X.T., Walton, A.J., & Fu, Y.Q. (2014). High frequency microfluidic performance of $LiNbO_3$ and ZnO surface acoustic wave devices. *Journal of Applied Physics*, *116*, 024501.
Heris, S.Z., Etemad, S., & Esfahany, M.N. (2006). Experimental investigation of oxide nanofluids laminar flow convective heat transfer. *International Communications in Heat and Mass Transfer*, *33*, 529–535.
Hsieh, S.-S., Hsu, Y.-F., & Wang, M.-L. (2014). A microspray-based cooling system for high powered leds. *Energy Conversion Management*, *78*, 338–346.
Huang, Y. -L., Chang, S. -H., Wang, C. -H., Lee, C. -I. (Eds.) (2005). *ASME2005 Summer Heat Transfer Conference Collocated with the ASME2005 Pacific Rim Technical Conference and Exhibition on Integration and Packaging of MEMS, NEMS, and Electronics Systems*, Vol. 4. ASME: San Francisco, CA, USA.
Khaleduzzaman, S., Mahbubul, I., Shahrul, I., & Saidur, R. (2013). Effect of particle concentration, temperature and surfactant on surface tension of nanofluids. *International Communications in Heat and Mass Transfer*, *49*, 110–114.
Kim, J. (2007). Spray cooling heat transfer: The state of the art. *International Journal of Heat and Fluid Flow*, *28*, 753–767.
Lee, A., Sudau, K., Ahn, K.H., Lee, S.J., & Willenbacher, N. (2012). Optimization of experimental parameters to suppress nozzle clogging in inkjet printing. *Industrial and Engineering Chemistry Research*, *51*, 13195–13204.
Lim, E.W.C., Koh, S.H., Lim, L.K., Ore, S.H., Tay, B.K., Ma, Y., & Wang, C.-H. (2008). Experimental and computational studies of liquid aerosol evaporation. *Journal of Aerosol Science*, *39*, 618–634.
Lohse, D., Jeurissen, R., De Jong, J., Versluis, M., Wijshoff, H., Van DenBerg, M., & Reinten, H. (2008). Bubbles in piezoacoustic inkjet printing. *The Journal of Acoustical Society of America*, *123* 3557–3557.
Miyamoto, K., Nagatomo, S., Matsui, Y., & Shiokawa, S. (2002). Nonlinear vibration of liquid droplet by surface acoustic wave excitation. *Japanese Journal of Applied Physics*, *41*, 3465.
Narendran, N., & Gu, Y. (2005). Life of led-based white light sources. *Journal of Display Technology*, *1*, 167.
Nguyen, T.K., Nguyen, V.D., Seong, B., Hoang, N., Park, J., & Byun, D. (2014). Control and improvement of jet stability by monitoring liquid meniscus in electrospray and electrohydrodynamic jet. *Journal of Aerosol Science*, *71*, 29–39.
Özerinç, S., Kakaç, S., & Yazcoğlu, A. (2010). Enhanced thermal conductivity of nanofluids: A state-of-the-art review. *Microfluidics and Nanofluidics*, *8*, 145–170.
Qi, A., Friend, J.R., Yeo, L.Y., Morton, D.A.V., McIntosh, M.P., & Spiccia, L. (2009). Miniature inhalation therapy platform using surface acoustic wave microfluidic atomization. *Lab on a Chip*, *9*, 2184–2193.
Qi, A., Yeo, L.Y., & Friend, J.R. (2008). Interfacial destabilization and atomization driven by surface acoustic waves. *Physics of Fluids*, *20*, 074103.
Rajapaksa, A., Qi, A., Yeo, L.Y., Coppel, R., & Friend, J.R. (2014). Enabling practical surface acoustic wave nebulizer drug delivery via amplitude modulation. *Lab on a Chip*, *14*, 1858–1865.
Ramachandran, V., & Fogler, H.S. (1999). Plugging by hydrodynamic bridging during flow of stable colloidal particles within cylindrical pores. *Journal of Fluid Mechanics*, *385*, 129–156.
Rezk, A.R., Manor, O., Friend, J.R., & Yeo, L.Y. (2012). Unique fingering instabilities and soliton-like wave propagation in thin acoustowetting films. *Nature Communications*, *3*, 1167.
Sen, A., Darabi, J., & Knapp, D. (2007). Simulation and parametric study of a novel multi-spray emitter for esims applications. *Microfluidics and Nanofluidics*, *3*, 283–298.
Shilton, R., Tan, M.K., Yeo, L.Y., & Friend, J.R. (2008). Particle concentration and mixing in microdrops driven by focused surface acoustic waves. *Journal of Applied Physics*, *104*, 014910.
Shilton, R.J., Travagliati, M., Beltram, F., & Cecchini, M. (2014). Nanoliter-droplet acoustic streaming via ultra high frequency surface acoustic waves. *Advanced Materials*, *26*, 4941–4946.
Tan, M.K., Friend, J.R., & Yeo, L.Y. (2007). Microparticle collection and concentration via a miniature surface acoustic wave device. *Lab on a Chip*, *7*, 618–625.
Tan, M.K., Friend, J.R., & Yeo, L.Y. (2009). Interfacial jetting phenomena induced by focused surface vibrations. *Physical Review Letters*, *103*, 024501.
Taylor, G. (1964). Disintegration of water drops in an electric field. *Proceedings of The Royal Society A*, *280*, 383–397.

Wang, H.-C., & Mamishev, A.V. (2012a). Heat transfer correlation models for electrospray evaporative cooling chambers of different geometry types. *Applied Thermal Engineering*, *40*, 91–101.
Wang, H.-C., & Mamishev, A.V. (2012b). Optimization methodology for electrospray evaporative cooling chambers. *Journal of Electrostatics*, *70*, 384–392.
Wilhelm, O., Mdler, L., & Pratsinis, S. (2003). Electrospray evaporation and deposition. *Journal of Aerosol Science*, *34*, 815–836.
Wu, T.-T., & Chang, I.-H. (2005). Actuating and detecting of microdroplet using slanted finger interdigital transducers. *Journal of Applied Physics*, *98*, 024903.
Zhang, Z., Jiang, P.-X., Ouyang, X.-L., Chen, J.-N., & Christopher, D.M. (2014). Experimental investigation of spray cooling on smooth and micro-structured surfaces. *International Journal of Heat and Mass Transfer*, *76*, 366–375.
Zhu, D. S., Wu, S. Y., & Wang, N. (2010). Surface tension and viscosity of aluminum oxide nanofluids. In *AIP Conference Proceedings*, Vol. *1207*, pp. 460–464.